

Time dependent signatures of core-collapse supernova neutrinos at HALO

B. Ekinci,^{1,*} Y. Pehlivan,^{1,†} and Amol V. Patwardhan^{2,‡}

¹*Mimar Sinan Fine Arts University, Sisli, Istanbul, 34380, Turkey*

²*SLAC National Accelerator Laboratory, 2575 Sand Hill Road, Menlo Park, CA, 94025*

(Dated: February 16, 2021)

We calculate the response of a lead-based detector, such as the Helium and Lead Observatory (HALO) or its planned upgrade HALO-1kt to a galactic core-collapse supernova. We pay particular attention to the time dependence of the reaction rates. All reaction rates decrease as the neutrino luminosity exponentially drops during the cooling period but the ratio of one-neutron (1n) to two-neutron (2n) event rates in HALO is independent of this overall decrease. Nevertheless, we find that this ratio still changes with time due to the changing character of neutrino flavor transformations with the evolving conditions in the supernova. In the case of inverted hierarchy, this is caused by the fact that the spectral splits become less and less sharp with the decreasing luminosity. In the case of normal hierarchy, it is caused by the passage of the shock wave through the Mikheyev-Smirnov-Wolfenstein resonance region. However, in both cases, we find that the change in the ratio of 1n to 2n event rates is limited to a few percent.

PACS numbers: 14.60.Pq, 95.85.Ry, 97.60.Bw, 95.55.Vj

Keywords: Core collapse supernova, neutrino detection, HALO, collective neutrino oscillations.

I. INTRODUCTION

Based on statistical and observational studies, somewhere between 0.5–3 supernova explosions should happen in our galaxy per century [1, 2]. The latest supernova exploded about 120 years ago [3] but it was not optically detected because it was buried in dust near the galactic center. However, with today’s neutrino detection capabilities, the next galactic core-collapse supernova will leave thousands of events in the neutrino detectors [4, 5] even if it explodes near the center of the galaxy. The question of what we can learn about the core-collapse supernovae and about neutrinos themselves from such a signal is a prevailing one. A recent review can be found in Ref. [6].

In this paper we are interested in calculating the response of a lead-based detector such as HALO or HALO-1kt to a galactic core-collapse supernova.¹ Neutrinos and antineutrinos of all flavors are emitted from a supernova [7, 8]. These neutrinos undergo flavor evolution after they thermally decouple from the proto-neutron star at the center. Besides the ordinary vacuum oscillations, this involves collective neutrino oscillations which happen due to coherent neutrino-neutrino scattering in the inner regions [9–12], and Mikheyev-Smirnov-Wolfenstein (MSW) resonances due to coherent scattering on background electrons [13–15] in the outer regions. HALO can detect these neutrinos through charged-current (CC) reactions

$$\begin{aligned} \nu_e + {}^{208}\text{Pb} &\longrightarrow {}^{207}\text{Bi} + n + e^-, \\ \nu_e + {}^{208}\text{Pb} &\longrightarrow {}^{206}\text{Bi} + 2n + e^-, \end{aligned} \quad (1)$$

and neutral-current (NC) reactions

$$\begin{aligned} \bar{\nu} + {}^{208}\text{Pb} &\longrightarrow {}^{207}\text{Pb} + n + \bar{\nu}, \\ \bar{\nu} + {}^{208}\text{Pb} &\longrightarrow {}^{206}\text{Pb} + 2n + \bar{\nu}, \end{aligned} \quad (2)$$

on 79 tons of ${}^{208}_{82}\text{Pb}$ target [16]. HALO-1kt will use 1 kiloton of lead target and will have significantly increased efficiency. All neutrino and antineutrino flavors can participate in NC reactions as indicated by the (–) overset in Eq. (2). As a result, these reactions are insensitive to flavor transformations. But the CC reactions can only be participated by electron neutrinos. Since ${}^{208}\text{Pb}$ is a neutron-rich nucleus, reactions with electron antineutrinos are suppressed by Pauli blocking. As a result, HALO is primarily sensitive to the flavor transformations of electron neutrinos inside the supernova. Currently, neutrino-lead cross sections are not experimentally known. But theoretical calculations are carried out by several groups [17–22]. Estimates of expected event rates at HALO are based on such calculations [23–26].

The first detailed study of the HALO event rates which took neutrino flavor evolution into account was Ref. [24]. The primary interest of this study was to extract information about the neutrino energy spectra emitted during the cooling period of the supernova from the HALO signal. To be able to scan the large parameter space, the authors adopted an approach which is based on modifying the neutrino energy spectra manually to mimic the dynamical flavor evolution. In particular, based on the results from earlier flavor evolution studies they assumed that sharp spectral swaps [27–33] occur in fixed parts of the neutrino energy spectra due to collective neutrino oscillations. They also ignored the effects of the shock wave. This practical approach allowed them to write down analytical expressions for the neutrino spectra reaching Earth for a large variety of initial conditions, and show that HALO signal can be used to extract information about the spec-

* Corresponding author: baekinci@gmail.com

† yamac.pehlivan@msgsu.edu.tr

‡ apatward@slac.stanford.edu

¹ From now on to be referred simply as a supernova.

tral pinching parameters. A similar approach was adopted in Ref. [25] which was concerned with determining the neutrino mass hierarchy by combining the electron neutrino signal from a lead or iron detector and the electron antineutrino signal from a water-Cherenkov detector. A complementary study was carried out more recently in Ref. [26], in which the authors used time dependent neutrino luminosities and initial energy distributions taken from a proto-neutron star simulation [34]. Since this simulation produced very similar fluxes for different flavors, and their primary purpose was to compare lead vs iron-based detectors in terms of total number of events, the authors ignored the collective neutrino oscillations and the effects shock wave.

This paper aims to estimate the event rates in HALO during a galactic supernova based on a fully *dynamical* and *time dependent* calculation of neutrino flavor evolution. Here, being *dynamical* refers to the explicit solutions of flavor evolution equations starting from the surface of the proto-neutron star and ending on the surface of the supernova. Collective oscillations and MSW resonances naturally appear in these dynamical solutions. The *time dependence* mentioned above refers to the fact that we include (i) the decreasing neutrino luminosity of the proto-neutron star during the cooling period and (ii) the propagating shock wave in the mantle.

During the cooling period, neutrino luminosities are expected to drop roughly as $L_{\nu_\alpha} e^{-t/\tau}$ [35, 36]. Here, t denotes the post-bounce time, τ is the relevant time scale, ν_α with $\alpha = e, \mu, \tau$ denotes the neutrino flavor, and L_{ν_α} is the initial ν_α luminosity. This will lead to exponentially decreasing reaction rates in all detectors. However, there is a more subtle effect: with decreasing neutrino luminosity, collective neutrino oscillations change their character, especially in the case of inverted hierarchy (IH). Our calculations for IH indicate that initially, when the neutrino luminosity is large, the spectral swaps are sharp. In other words, completely adiabatic or diabatic transitions occur across the whole spectrum, depending on the energy. As the neutrino luminosity drops, we see partially adiabatic transitions in the part of the spectrum above 35 MeV. This is the part of the spectrum to which a lead-based detector is most sensitive, i.e., most of the neutrons produced in the detector will originate from neutrinos in this energy region [26]. Therefore, it is reasonable to ask whether this effect can lead to a time dependence beyond the exponential drop in reaction rates in the case of IH. In the case of normal hierarchy (NH), collective oscillations affect only the very low energy part of the spectrum. For this reason, one does not expect to see a similar effect for NH.

The second source of time dependence in the HALO signal is the propagating shock wave. This effect can be expected to appear when the shock wave reaches the MSW resonance region. There are two MSW resonances: The low resonance occurs in the outermost layers of the mantle and is experienced by neutrinos in both NH and IH. However, one does not expect to see its effect in

reaction rates because the shock wave reaches there at very late times when the neutrino luminosity drops to a few percent of its initial value. The high resonance occurs at relatively higher densities and is experienced by neutrinos only in the case of NH. The shock wave reaches this region relatively earlier, while there is still a sizable neutrino luminosity. Therefore, in principle, it is possible to see the effects of the shock wave in reaction rates in the case of NH.

The impact of the supernova shock waves on neutrino flavor evolution has been examined in several works over the years [37–44]. The combined effect of the collective neutrino oscillations and the shock wave modification of MSW resonances was first considered in Ref. [43]. In this work, an interesting interplay between the two features was pointed out for electron antineutrinos which feel both effects in the case of IH. This has observational consequences for water-Cherenkov and liquid scintillator experiments. However, no such interplay is to be expected in the HALO signal: HALO is sensitive to the flavor evolution of electron neutrinos only, and they are affected either by collective oscillations in the case of IH, or by the shock wave modification of MSW resonances in the case of NH. This separation of effects is one of the motivations of the present study.

Another motivation is the fact that HALO has an adequate timing mechanism to look for dynamical effects in a supernova. It has a time resolution of about 200 μ s, which is the time required for the emitted neutrons to thermalize before being captured at the ^3He counters [45, 46]. In addition, all events are time stamped by a GPS-based system [46], allowing a comparison with other neutrino observatories.

Our treatment covers neither the dynamical aspects of neutrino flavor evolution nor the time dependent features of the supernova neutrino signal fully. As for the dynamical flavor evolution, we leave out the multiangle nature of the collective neutrino oscillations: we treat the dependence of the neutrino-neutrino interactions on the angle between the neutrinos [47] in an effective way using the so-called *neutrino bulb model* [27]. The multiangle effects are expected to delay the onset of collective oscillations but leave its general features intact for the type of initial spectra that we consider [48]. We also do not take the time evolution of the proto-neutron star itself into account as is done, for example, in Ref. [26]. In reality, the radius of the proto-neutron star, and the energy distributions of the emitted neutrinos slightly change during the cooling period. See, for example, Refs. [35, 36]. Our purpose in leaving out this important feature is to isolate and examine the other time dependent features mentioned above.

We start in Section II with a general description of the neutrino flavor evolution equations in the supernova. In Section III, we provide a semi-analytical view of flavor evolution with an emphasis on the sharpness of spectral splits in terms of a simple jumping probability p between the matter eigenstates in the collective oscillation region. We

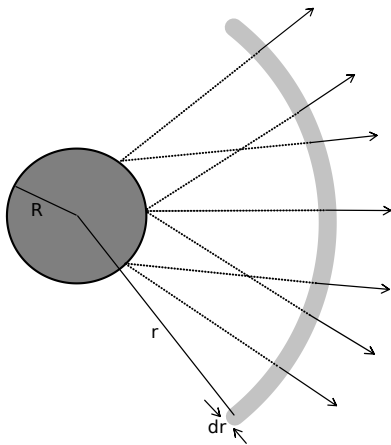


FIG. 1. Schematic picture of neutrino emission from the proto-neutron star and the neutrino ensemble represented by the density operator $\hat{\rho}_t(E, r)dtdE$ in the neutrino bulb model [27]. See the text for details.

present flavor evolution examples and show the departure from the sharp spectral splits in the high energy region. The discussion in this section is useful in interpreting our results in the case of IH. In Section IV, we calculate the expected reaction rates per kiloton of lead target for four different neutrino energy distribution models as a function of time. In particular we present the results for the time dependence of the ratio of 1n to 2n events. We present our conclusions in Section V.

II. SUPERNOVA NEUTRINOS

We assume that the supernova is spherically symmetric, and that neutrinos of all flavors and energies thermally decouple at a single sharp surface close to the surface of the proto-neutron star. After that, neutrinos freely stream uniformly in all directions. This is known as the *neutrino bulb model*, which was developed in Ref. [27]. We also adopt the single-angle approximation in describing the neutrino flavor evolution. Both of these approaches are summarized below.

Let us consider all neutrinos with energy between E and $E + dE$ which are emitted from the surface of the proto-neutron star during a post-bounce time interval between t and $t + dt$. Not all of these neutrinos travel radially because emission can happen in any angle from the surface of the proto-neutron star. (See Fig. 1.) But, in the single angle approximation, it is assumed that these neutrinos reach a given distance (say r) from the center of the supernova at the same time. In other words, small differences in their paths are omitted. Furthermore, the single angle approximation and the spherical symmetry assumption together imply that any two neutrinos in this group evolve in the same way regardless of their direction,

provided that they are initially emitted in the same flavor. Therefore, these neutrinos form an ensemble which evolves with distance r . Here we choose to work with *unnormalized* density operators, i.e., we want to define an infinitesimal density operator $\hat{\rho}_t(E, r)dtdE$ whose trace is equal to the *total* number of neutrinos with energy between E and $E + dE$, emitted from the proto-neutron star between t and $t + dt$. These neutrinos occupy the shaded region between r and $r + dr$ shown in Fig. 1 at a later time. Here, we use the natural units so that $dr = dt$.

On the surface of the proto-neutron star where $r = R$, this density operator is given by

$$\hat{\rho}_t(E, R) = \sum_{\alpha=e,\mu,\tau} \frac{L_{\nu_\alpha} e^{-t/\tau}}{\langle E_{\nu_\alpha} \rangle} f_{\nu_\alpha}(E) |\nu_\alpha\rangle \langle \nu_\alpha|. \quad (3)$$

The above equation is easy to understand: $L_{\nu_\alpha} e^{-t/\tau}$ is the total energy emitted per unit time in terms of ν_α 's. Dividing this by their average energy $\langle E_{\nu_\alpha} \rangle$, we find the number of ν_α 's emitted per unit time. Finally, multiplication with their normalized energy distribution $f_{\nu_\alpha}(E)$ yields the number of those ν_α 's per unit energy interval. For antineutrinos, we define an analogous expression $\hat{\rho}_t(E, R)$ which is the same as in Eq. (3) except that neutrino quantities are replaced with antineutrino quantities labeled by $\bar{\nu}_\alpha$, e.g., $L_{\bar{\nu}_\alpha}$, $\langle E_{\bar{\nu}_\alpha} \rangle$, etc ...

The neutrino luminosities used in Eq. (3) can be found from the total binding energy E_B emitted by the supernova. Since almost all of this energy is emitted in terms of neutrinos during the cooling period, divided equally between all neutrino and antineutrino flavors, neutrino luminosities can be calculated from $E_B = 6 \times \int_0^\infty L_{\nu_\alpha} e^{-t/\tau} dt$. In our simulations, we use $\tau = 3$ s [35, 36]. We take the total released gravitational binding energy as $E_B = 5.72 \times 10^{53}$ ergs, which is close to the upper limit² of the binding energy released by the SN1987A as calculated from the observed $\bar{\nu}_e$ signal [51]. This leads to the initial neutrino luminosities given by $L_{\nu_\alpha} = L_{\bar{\nu}_\alpha} = 3.18 \times 10^{52}$ erg/s, which drops exponentially after that.

Unlike the luminosities, the energy distributions of different neutrino and antineutrino flavors are not the same because they are subject to different interactions inside the proto-neutron star. Here we adopt the fit function provided by Ref. [52] by setting their dimensionless fitting parameter to 3 and normalizing accordingly, which gives

$$f_{\nu_\alpha}(E) = \frac{128E^3}{3\langle E_{\nu_\alpha} \rangle^4} \exp\left(-\frac{4E}{\langle E_{\nu_\alpha} \rangle}\right). \quad (4)$$

Simulations of neutrino transport in proto-neutron star generally lead to average energies around 10-20 MeV. (See Ref. [53] for a partial compilation of these simulations

² Note that the observed mass of the residual neutron star mass suggests a more conservative range of 1.0×10^{53} ergs $< E_B < 4.0 \times 10^{53}$ ergs [49]. Also see the discussion in Ref. [50].

Supernova	
Initial neutrino luminosities: $L_{\nu_\alpha} = L_{\bar{\nu}_\alpha} = 3.18 \times 10^{52}$ erg/s	
Decay time $\tau = 3.0$ s	
Total energy released: $E_B = 5.72 \times 10^{53}$ erg	
Neutron star radius: $R = 10$ km	
Distance to Earth: $d = 10$ kpc	
Average energies	
Model I: $\langle E_{\nu_e} \rangle = 8$ MeV $\langle E_{\bar{\nu}_e} \rangle = 11$ MeV $\langle E_{\nu_x} \rangle = 13$ MeV	
Model II: $\langle E_{\nu_e} \rangle = 8$ MeV $\langle E_{\bar{\nu}_e} \rangle = 11$ MeV $\langle E_{\nu_x} \rangle = 16$ MeV	
Model III: $\langle E_{\nu_e} \rangle = 8$ MeV $\langle E_{\bar{\nu}_e} \rangle = 11$ MeV $\langle E_{\nu_x} \rangle = 20$ MeV	
Model IV: $\langle E_{\nu_e} \rangle = 15$ MeV $\langle E_{\bar{\nu}_e} \rangle = 20$ MeV $\langle E_{\nu_x} \rangle = 25$ MeV	
Neutrino Mixing	
$\sin \theta_{12} = 0.554$ $\sin \theta_{13} = 0.148$ $m_2^2 - m_1^2 = 7.53 \times 10^{-5} \text{eV}^2$	
$\sin \theta_{23} = 0.715$ $m_3^2 - m_2^2 = 2.44 \times 10^{-3} \text{eV}^2$ (for NH)	
$\sin \theta_{23} = 0.732$ $m_3^2 - m_2^2 = -2.55 \times 10^{-3} \text{eV}^2$ (for IH)	
Detector	
Mass = 1 kt	
Reactions and threshold energies	
$\nu_e + {}^{208}\text{Pb} \rightarrow {}^{207}\text{Bi} + n + e^-$	$E_{\text{th}} = 9.76$ MeV
$\nu_e + {}^{208}\text{Pb} \rightarrow {}^{206}\text{Bi} + 2n + e^-$	$E_{\text{th}} = 17.86$ MeV
$\bar{\nu} + {}^{208}\text{Pb} \rightarrow {}^{207}\text{Pb} + n + \bar{\nu}$	$E_{\text{th}} = 7.37$ MeV
$\bar{\nu} + {}^{208}\text{Pb} \rightarrow {}^{206}\text{Pb} + 2n + \bar{\nu}$	$E_{\text{th}} = 14.11$ MeV

TABLE I. The summary of the parameters that we use in our numerical calculations.

and the references therein.) In this paper, we use four different sets of average energies which are referred to as models I-IV in Table I. We choose these particular sets of average energies in order to cover qualitatively different scenarios as discussed in the next section.

As the neutrinos move outward, the density operator representing our ensemble changes according to

$$\frac{d}{dr} \hat{\rho}_t(E, r) = -i[\hat{H}_t(E, r), \hat{\rho}_t(E, r)]. \quad (5)$$

Here we use r as the proper time of the neutrinos because they propagate almost with the speed of light. As they quickly fly through the supernova, they essentially see the background as it is when they are emitted at time t . This is because most of the non-trivial flavor evolution (collective effects and the MSW resonances) occurs before 10^5 km, and it takes only a fraction of a second for the neutrinos to reach there. For this reason, we use the Hamiltonian $H_t(E, r)$ which represents the conditions in the supernova at time t to describe the evolution of $\hat{\rho}_t(E, r)$. This Hamiltonian is given by

$$\begin{aligned} \hat{H}_t(E, r) = & \sum_i \frac{m_i^2}{2E} |\nu_i\rangle \langle \nu_i| + \sqrt{2} G_F N_e(t, r) |\nu_e\rangle \langle \nu_e| \\ & + \frac{\sqrt{2} G_F}{2\pi R^2} D\left(\frac{R}{r}\right) \int (\hat{\rho}_t(E', r) - \hat{\rho}_t(E', r)) dE'. \end{aligned} \quad (6)$$

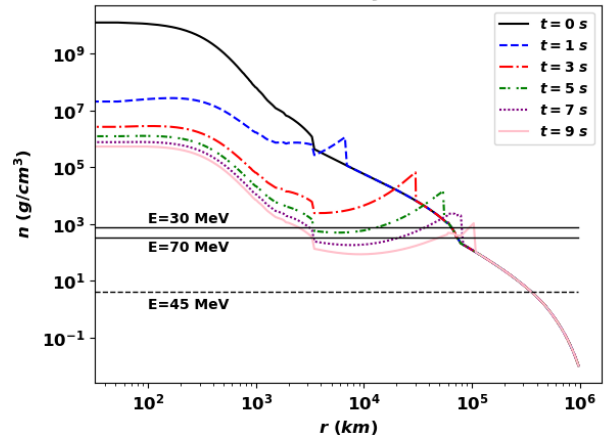


FIG. 2. The density for the progenitor model and various post-bounce times. The solid horizontal lines represent the high resonance densities for 30 MeV and 70 MeV neutrinos. The dashed horizontal line represents the low resonance density for a 45 MeV neutrino.

Here, the first term represents the vacuum oscillations. ν_i is the eigenstate of mass m_i for $i = 1, 2, 3$, which is related to the flavor eigenstates via $\langle \nu_\alpha | \nu_i \rangle = U_{\alpha i}$ where U is the neutrino mixing matrix [54]. Subtracting the trace of this term from the Hamiltonian allows one to use only mass squared differences given in Table I.

The second term in Eq. (6) represents the CC forward scattering of neutrinos from the background electrons and protons [13, 55] with G_F denoting the Fermi interaction constant and $N_e(t, r)$ denoting the net electron number density at radius r at time t . Assuming that the number of electrons per baryon is equal to 0.5, electron number density $N_e(t, r)$ is related to the mass density $n(t, r)$ by

$$N_e(t, r) = \left(\frac{n(t, r)}{10^8 \text{g/cm}^3} \right) 3.01 \times 10^{31} \text{cm}^{-3}. \quad (7)$$

At $t = 0$, we use the mass density profile provided by Ref. [56] as a $6M_\odot$ helium-core progenitor model for SN1987A. This profile is shown in Fig. 2 with the solid black line. For post-bounce times, we obtain the density profile by superimposing a parametric shock wave on the progenitor profile as described in Ref. [38]. The resulting post-bounce density profiles for $t = 1, 3, 5, 7$ s are also shown in Fig. 2.

The last term in Eq. (6) represents the NC forward and exchange scatterings of neutrinos from each other [9, 10, 47, 57, 58]. The energy integral contains all neutrinos at radius r . This may be confusing because it appears to imply that every neutrino in the ensemble with energy E meets and interacts with every other neutrino in the whole system. However, this is not the case. According to the neutrino bulb model, a *test neutrino* interacts only with those neutrinos which cross its path. But due to the assumption of spherical symmetry and the single angle approximation, the evolution of the ones that it meets is

the same as those that it does not. As a result, one can use the density operator of the whole system by simply multiplying it with a geometrical factor which yields its relevant fraction. This geometrical factor is $\frac{1}{2\pi R^2} D\left(\frac{R}{r}\right)$ with [27]

$$D\left(\frac{r}{R}\right) = \frac{1}{2} \left[1 - \sqrt{1 - \left(\frac{R}{r}\right)^2} \right]^2. \quad (8)$$

This factor also takes care of the angle dependence of the neutrino-neutrino interactions in an effective way. The density operator $\hat{\rho}_t(E, r)$ which appears the energy integral represents the antineutrinos in an analogous way to neutrinos. Antineutrino density operators undergo the same evolution except that their Hamiltonian should be obtained from Eq. (6) by interchanging neutrino and antineutrino degrees of freedom and reversing the sign of the CC interaction term. We do not consider any charge-parity violations here because it would have no affect on the HALO signal.³

III. FLAVOR EVOLUTION

A. Collective Oscillations

It is helpful to describe the neutrino flavor evolution in the *matter basis*, which instantaneously diagonalizes the Hamiltonian. Since the Hamiltonian changes with distance, so does the matter basis. We find it useful to denote the matter basis at distance r from the center of the supernova with $|r_i\rangle$ where $i = 1, 2, 3$ orders the matter eigenvalues from the lightest to the heaviest. In other words, we write the Hamiltonian given in Eq. (6) as

$$H(r) = \sum_{i=1}^3 \mathcal{E}_i(r) |r_i\rangle\langle r_i|, \quad (9)$$

where $\mathcal{E}_1(r) < \mathcal{E}_2(r) < \mathcal{E}_3(r)$ is satisfied. For simplicity, we drop the time and energy dependence of the Hamiltonian and the density operator from our notation in the rest of the paper. Since the Hamiltonian depends on the post-bounce time and the energy of the neutrino, so do its eigenvalues and eigenstates on the right hand side of Eq. (9). But this dependence is similarly suppressed in our notation.

For the models that we consider, we have

$$\begin{aligned} |R_1\rangle &\approx \sin\theta_{23}|\nu_\mu\rangle + \cos\theta_{23}|\nu_\tau\rangle, \\ |R_2\rangle &\approx \cos\theta_{23}|\nu_\mu\rangle - \sin\theta_{23}|\nu_\tau\rangle, \\ |R_3\rangle &\approx |\nu_e\rangle, \end{aligned} \quad (10)$$

³ This statement is true as long as $\nu_\mu, \nu_\tau, \bar{\nu}_\mu, \bar{\nu}_\tau$ have the same emission spectra [59–63], and as long as the neutrino magnetic moment is small [64].

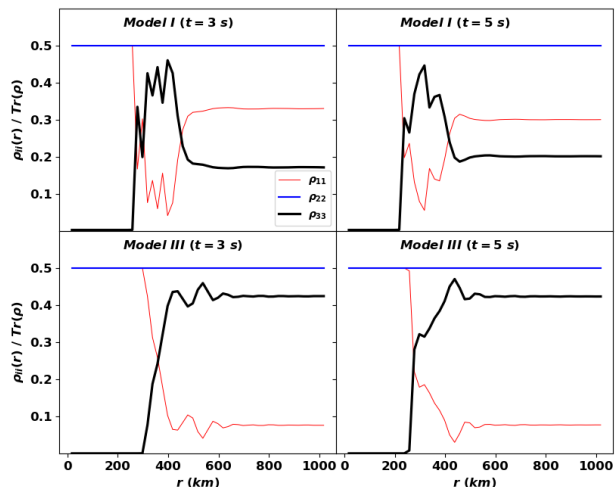


FIG. 3. The decoupling of the second matter eigenstate from the dynamics during collective oscillations. The plot shows the diagonal elements of the density operator in matter basis (i.e., $\rho_{ii}(r) = \langle r_i | \hat{\rho}(r) | r_i \rangle$) divided by its trace. The thick black line corresponds to the heaviest matter eigenstate which mixes with the lightest shown with the thin red line. The blue line with medium thickness shows the second matter eigenstate which decouples from the dynamics. This is for a 45 MeV neutrino in IH for models I and III at 3 s and 5s. For other models, energies, and times the results are similar.

on the surface of the proto-neutron star where $r = R$. Since the luminosities are equal and the ν_μ and ν_τ energy distributions are the same, the initial density operator given in Eq. (3) can be written in the matter basis as

$$\hat{\rho}(R) = \rho_{\mu\mu}(R) (|R_1\rangle\langle R_1| + |R_2\rangle\langle R_2|) + \rho_{ee}(R) |R_3\rangle\langle R_3|. \quad (11)$$

Here the flavor components $\rho_{\alpha\alpha}(R)$ are defined in Eq. (3). For the models that we consider, collective oscillations mix the first and third matter eigenstates while the second mass eigenstate decouples from the dynamics. Examples of this behavior are shown in Fig. 3. This behavior is expected based on the results of earlier studies, such as those in Refs. [33]. This tells us that 12 and 23 elements of the evolution operator in the matter basis are zero whereas its 13 component can be parametrized as

$$\langle r_1 | \mathcal{U}(r, R) | R_3 \rangle = \sqrt{p} e^{i\delta(r)}. \quad (12)$$

Here, $\mathcal{U}(r, R)$ denotes the evolution operator from R to r , and p is the probability of $|R_3\rangle \leftrightarrow |r_1\rangle$ transition. Both p and the phase $\delta(r)$ depend on the neutrino energy and the post-bounce time. But p depends on the distance only for a short period during the collective oscillations. Once the collective oscillations end at about 500 km, p is independent of distance (see Fig. 3). However the phase $\delta(r)$ depends on the distance r due to the $\exp(-i \int \mathcal{E}_i(r) dr)$ terms picked up by the instantaneous eigenstates during the evolution. As a result, after the collective oscillations

end the density operator is given by

$$\begin{aligned} \hat{\rho}(r) = & ((1-p)\rho_{\mu\mu}(R) + p\rho_{ee}(R))|r_1\rangle\langle r_1| \\ & + \rho_{\mu\mu}(R)|r_2\rangle\langle r_2| \\ & + (p\rho_{\mu\mu}(R) + (1-p)\rho_{ee}(R))|r_3\rangle\langle r_3| \\ & + \sqrt{p(1-p)}\left(\rho_{ee}(R)e^{i\delta(r)} - \rho_{\mu\mu}(R)e^{-i\delta(r)}\right)|r_1\rangle\langle r_3| \\ & + \text{h.c.} \end{aligned} \quad (13)$$

Here h.c. stands for hermitian conjugate of the $|r_1\rangle\langle r_3|$ term. The exponential phase terms cancel each other in the diagonal terms of the density operator, but they do appear in the non-diagonal terms.

Eq. (13) is true for both NH and IH, but with different crossing probabilities. In the case of NH, the collective oscillations create a spectral swap in the low energy part of the spectrum below a split energy E_{NH} . In the case of IH, they create a spectral swap between a low and a high split energy, denoted, respectively, by E_{IH} and E'_{IH} . In the ideal case of a *sharp split*, p is equal to 1 in the swapped region and 0 in the unswapped region. In other words, in the case of a sharp split one expects to find

$$p \approx \begin{cases} 1 & \text{for } E < E_{\text{NH}} \\ 0 & \text{for } E > E_{\text{NH}} \end{cases} \quad \text{in NH,} \quad (14)$$

and

$$p \approx \begin{cases} 1 & \text{for } E_{\text{IH}} < E < E'_{\text{IH}} \\ 0 & \text{otherwise} \end{cases} \quad \text{in IH.} \quad (15)$$

NH spectral swap happens in the very low energy part of the spectrum. For all the models that we considered, E_{NH} was lower than all the reaction threshold energies, which are listed in Table I. But the IH swap occurs in the region to which HALO is most sensitive. For the models I-III, the low split energy E_{IH} is around 7-9 MeV. This is close to, but lower than, the CC1n reaction threshold, which is 9.76 MeV. In order to see the effects of an IH low split energy which is higher than this threshold, we set up the fourth model with higher average energies. In model IV, we find $E_{\text{IH}} = 14$ MeV, which is higher than the CC1n reaction threshold but lower than the CC2n reaction threshold. The high split energy E'_{IH} steadily increases as we go from model I to model IV. For model I, it is 35 MeV, and for model IV, it is 60 MeV. It also increases slightly with time within each model.

In the IH case, spectral splits are not sharp in the high energy region of the spectrum. At high energies, the jumping probability p takes values between 0 and 1 as shown in Fig. 4. In this figure, we show the jumping probability p for models I-IV as a function of energy at even times. In earlier times, the spectral swap is closer to being sharp with $p \approx 0.1$ in the high energy region. But at later times, the splits become less and less sharp.

The departure from a sharp spectral split manifests itself most notably in the oscillations of the diagonal density operator components in flavor basis. This can be

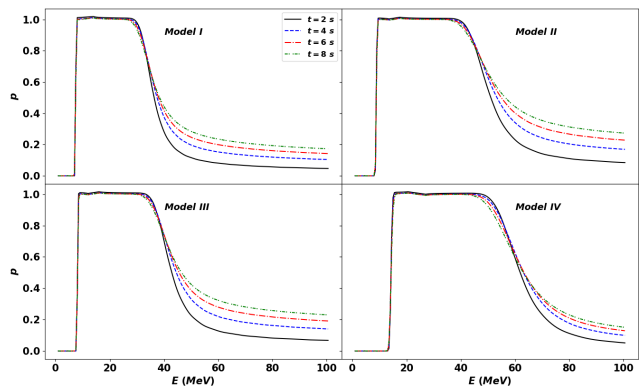


FIG. 4. The jumping probability p defined in Eq. (12) for models I-IV calculated as a function of energy at even seconds. At earlier times, the spectral swap is closer to being sharp. But at later times, the splits become less and less sharp in the high energy region.

seen by taking the expectation values of $\hat{\rho}(r)$ given in Eq. (13) between the flavor states ν_α , which leads to

$$\begin{aligned} \rho_{\alpha\alpha}(r) = & ((1-p)\rho_{\mu\mu}(R) + p\rho_{ee}(R))|\langle\nu_\alpha|r_1\rangle|^2 \\ & + \rho_{\mu\mu}(R)|\langle\nu_\alpha|r_1\rangle|^2 \\ & + (p\rho_{\mu\mu}(R) + (1-p)\rho_{ee}(R))|\langle\nu_\alpha|r_3\rangle|^2 \\ & + 2\sqrt{p(1-p)}(\rho_{ee}(R) - \rho_{\mu\mu}(R))|\langle\nu_\alpha|r_1\rangle\langle r_3|\nu_\alpha\rangle|\cos\delta(r). \end{aligned} \quad (16)$$

As the neutrinos move through the star, the projections of matter eigenstates on flavor eigenstates (i.e. $\langle\nu_\alpha|r_i\rangle$) change slowly. As a result, $\rho_{\alpha\alpha}(r)$ has a smooth variation described by the first three terms of the equation above. However, the last term gives rise to fast oscillations if p is different from 0 or 1. An example of this behavior is shown in Fig. 5 where we plot $\rho_{\alpha\alpha}(r)$ for a neutrino with 45 MeV energy in IH for models I and III at $t = 3$ s and $t = 5$ s. Notice that the amplitude of the oscillations grows in each case as the neutrino propagates. This is due to the $\langle\nu_\alpha|r_1\rangle\langle r_3|\nu_\alpha\rangle$ term in the last line of Eq. (16). In the inner regions where the electron density is high, $|\nu_e\rangle$ is practically the heaviest matter eigenstate. In other words, we have $\langle\nu_e|r_3\rangle \approx 1$, $\langle\nu_e|r_1\rangle \approx 0$, and $\langle\nu_{\mu,\tau}|r_3\rangle \approx 0$. As a result, the oscillation amplitudes do not grow until the density drops and ν_e starts to have a projection on lighter matter eigenstates. These oscillations are akin to the *phase effects* first discussed in Ref. [41].

B. MSW Resonances

Neutrino-neutrino interactions become negligible after a few hundred kilometers from the center. In our simulations, we manually turn off the neutrino-neutrino interaction term at 1000 km, after which the Hamiltonian contains only the vacuum oscillations and the effects of the other background particles. The evolution of neutrinos under these conditions is well understood in terms

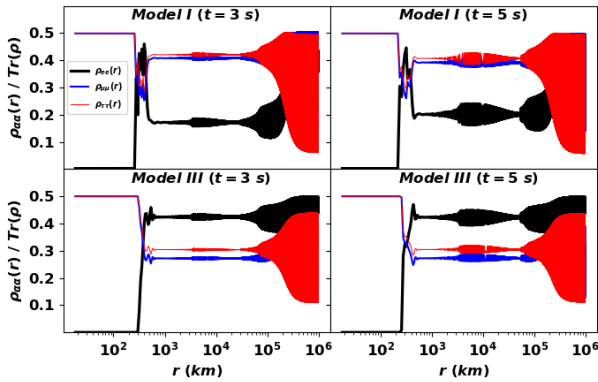


FIG. 5. The oscillations of the diagonal elements of the density operator in flavor basis due to the partial adiabaticity of collective oscillations. These examples show a 45 MeV neutrino in IH for models I and III at 3 s and 5 s. For other models, energies, and times, the behavior is similar.

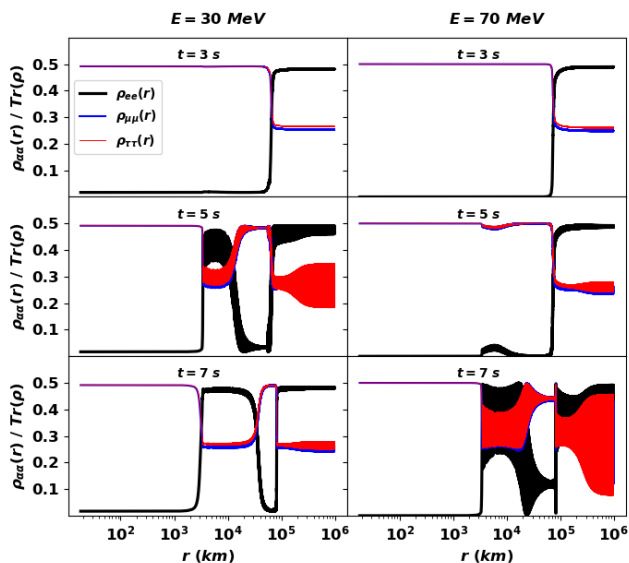


FIG. 6. The evolution of 30 MeV (left panels) and 70 MeV (right panels) neutrinos in the case of NH for model I at 3 s, 5 s, and 7 s. At earlier times, neutrinos go through one adiabatic high resonance. At later times, they go through three high resonances, and the adiabaticity is temporarily broken for each energy.

of the MSW resonances [13, 14]. As long as the density profile changes slowly in comparison to the neutrino oscillation wavelengths, the flavor evolution is adiabatic, i.e., the dynamical evolution of each matter eigenstate follows its own slow change with the background density [15]. At the resonant densities, the flavor content of matter eigenstates change very fast and the adiabaticity is easiest to break.

In the case of NH, neutrinos first go through the high

resonance. The horizontal lines in Fig. 2 show the high resonance densities for 30 MeV and 70 MeV neutrinos for illustration. A resonance occurs where they cross the supernova density profile. At earlier times, neutrinos experience only one high resonance, but at later times multiple high resonances occur due to the low density region between the front shock and the reverse shock. The resulting flavor evolutions are shown in Fig. 6 for 30 MeV (left panels) and 70 MeV (right panels) neutrinos at $t = 3$ s, (upper panels) $t = 5$ s (middle panels), and $t = 7$ s (lower panels) for model I in the case of NH. The neutrinos are not affected by collective oscillations in the inner regions. At $t = 3$ s, both neutrinos experience only one adiabatic high resonance transformation around 10^5 km. At $t = 5$ s, the 30 MeV neutrino goes through three resonances. The effects of the first and second resonances mostly cancel each other. In other words, after the second resonance, $\rho_{\alpha\alpha}(r)$ come close to their pre-resonance values. However, the adiabaticity is broken as evidenced by the presence of the oscillations.⁴ At $t = 5$ s, the density is close but not yet equal to the resonance value for 70 MeV neutrino in between the front and the reverse shock. This creates the small bumps in middle right panel. But, other than that, this neutrino goes through its regular adiabatic high resonance as it did at $t = 3$ s. At $t = 7$ s, 30 MeV neutrino still goes through three resonances but the first two resonances now completely cancel each other. The adiabaticity is also restored. For this neutrino, $\rho_{\alpha\alpha}$ values on the surface of the star are almost the same at $t = 3$ s and at $t = 7$ s. The 70 MeV neutrino also starts to go through three resonances at $t = 7$ s and its adiabaticity temporarily is broken.

This example illustrates the general behavior that we observe in all of our calculations in NH. The arrival of the shock wave to high MSW resonance region has only a limited effect on the neutrino survival probabilities. Instead of one high resonance, neutrinos go through three high resonances but, the first two resonances mostly cancel each other. Also the adiabaticity is initially violated but later restored. See Ref. [40] for a more in-depth discussion of the effects of the shock wave on the MSW resonances.

The low MSW resonance lies closer to the surface of the star, and it is experienced by neutrinos in both NH and IH. Fig. 2 shows the low resonance density value for a 45 MeV neutrino for illustration. In IH, its effect can be seen in Fig. 5 at around 5×10^5 km where ρ_{ee} starts to increase. We do not see the effect of low resonance in Fig. 6 because in NH it mainly causes transformations between ν_μ and ν_τ , which already evolved similarly up to that point. The low resonance is always adiabatic. The shock wave arrives at this region later than the 9 s mark, by which time the neutrino luminosity is already low, and we stop our calculations.

⁴ The argument is similar to the one presented above: When the adiabaticity is partially (but not completely) broken, an oscillation term appears in the last line of Eq. (16).

C. Approximate Degeneracy Between NH and IH

A degeneracy was reported in Ref. [24] between the total event counts in NH and IH cases. We find this to be approximately true. The source of this approximate degeneracy is easy to understand in light of the above discussion.

Since the low resonance is always adiabatic, Eq. (13) is valid through the surface of the star for IH with only the definitions of the matter eigenstates changing with distance. For NH, this is also the case if we assume that the first and the second high resonances perfectly cancel each other at later times and ignore the temporary violations of adiabaticity. Once the neutrinos reach the vacuum, we have

$$\begin{aligned} |r_1\rangle &= |\nu_1\rangle & |r_2\rangle &= |\nu_2\rangle & |r_3\rangle &= |\nu_3\rangle & \text{for NH,} \\ |r_1\rangle &= |\nu_3\rangle & |r_2\rangle &= |\nu_1\rangle & |r_3\rangle &= |\nu_2\rangle & \text{for IH.} \end{aligned} \quad (17)$$

Substituting this into Eq. (13), we find that their density operator is given by

$$\begin{aligned} \hat{\rho}(r) &= ((1-p)\rho_{\mu\mu}(R) + p\rho_{ee}(R))|\nu_1\rangle\langle\nu_1| \\ &+ \rho_{\mu\mu}(R)|\nu_2\rangle\langle\nu_2| \\ &+ (p\rho_{\mu\mu}(R) + (1-p)\rho_{ee}(R))|\nu_3\rangle\langle\nu_3| \\ &+ \sqrt{p(1-p)}\left(\rho_{ee}(R)e^{i\delta(r)} - \rho_{\mu\mu}(R)e^{-i\delta(r)}\right)|\nu_1\rangle\langle\nu_3| \\ &+ \text{h.c.} \end{aligned} \quad (18)$$

for NH, and by

$$\begin{aligned} \hat{\rho}(r) &= ((1-p)\rho_{\mu\mu}(R) + p\rho_{ee}(R))|\nu_3\rangle\langle\nu_3| \\ &+ \rho_{\mu\mu}(R)|\nu_1\rangle\langle\nu_1| \\ &+ (p\rho_{\mu\mu}(R) + (1-p)\rho_{ee}(R))|\nu_2\rangle\langle\nu_2| \\ &+ \sqrt{p(1-p)}\left(\rho_{ee}(R)e^{i\delta(r)} - \rho_{\mu\mu}(R)e^{-i\delta(r)}\right)|\nu_3\rangle\langle\nu_2| \\ &+ \text{h.c.} \end{aligned} \quad (19)$$

for IH as they leave the star.

After the neutrinos leave the star, they travel a long distance to reach the Earth. Over such distances, one should take *neutrino decoherence* into account, which is the fact that the mass eigenstates traveling with different speeds open up a gap between them. For $r > r_{\text{coh}}$, the gap becomes larger than their wavepacket size, and they cease to overlap. After that, the off-diagonal terms of the density matrix in the mass basis decrease with $e^{-(r/r_{\text{coh}})^2}$. For supernova neutrinos, the coherence length is of the order of a fraction of a parsec. By the time the neutrinos travel 10 kpc, their density operator is given only by the diagonal components of those given in Eqs. (18) and (19). To calculate the detector response, we only need the ν_e component of the density operator, which is given by

$$\begin{aligned} \hat{\rho}_{ee}(d) &= ((1-p)\rho_{\mu\mu}(R) + p\rho_{ee}(R))U_{e1}^2 + \rho_{\mu\mu}(R)U_{e2}^2 \\ &+ (p\rho_{\mu\mu}(R) + (1-p)\rho_{ee}(R))U_{e3}^2 \end{aligned} \quad (20)$$

for NH and by

$$\begin{aligned} \hat{\rho}_{ee}(d) &= ((1-p)\rho_{\mu\mu}(R) + p\rho_{ee}(R))U_{e3}^2 + \rho_{\mu\mu}(R)U_{e1}^2 \\ &+ (p\rho_{\mu\mu}(R) + (1-p)\rho_{ee}(R))U_{e2}^2 \end{aligned} \quad (21)$$

for IH, where d is the distance between the Earth and the supernova.

Let us assume that sharp spectral splits develop as in Eqs. (14) and (15). The NH split energy E_{NH} is always lower than both of the IH split energies E_{IH} and E'_{IH} . Therefore, in the energy region $E_{\text{IH}} < E < E'_{\text{IH}}$ swapped by the collective oscillations, we have

$$\hat{\rho}_{ee}(d) \approx \rho_{ee}(R)U_{e3}^2 + \rho_{\mu\mu}(R)(1 - U_{e3}^2) \quad (22)$$

for both NH and IH. This formula can be found by substituting $p = 0$ in Eq. (20) and by substituting $p = 1$ in Eq. (21). One also needs to use the fact that $U_{e1}^2 + U_{e2}^2 + U_{e3}^2 = 1$. This leads to a near degeneracy between the NH and IH event rates because HALO is most sensitive in the energy region which is typically swapped by collective oscillations in the IH case. However the degeneracy is broken by several factors. This includes the departure from sharp spectral splits, and the reactions caused by neutrinos with energy higher than E'_{IH} .

IV. REACTION RATES

The flux of neutrinos of type ν_α with energy between E and $E + dE$ at Earth is given by⁵ $(1/4\pi d^2)\rho_{\alpha\alpha}(d)dE$. Therefore, the number of a particular kind of reaction per unit time per target nucleus is equal to

$$\lambda(t) = \frac{1}{4\pi d^2} \int_{E_{\text{th}}}^{\infty} \rho_{\alpha\alpha}(d)\sigma(E)dE. \quad (23)$$

Here $\sigma(E)$ and E_{th} denote the cross section and the threshold energy of the reaction, respectively. $\rho_{\alpha\alpha}(d)$ depends on the post-bounce time t and the neutrino energy E implicitly. If there are N target nuclei in the detector, the rate of this particular reaction is given by $N\lambda(t)$. For a detector of mass M , this is equal to

$$\begin{aligned} N\lambda(t) &= 241\text{s}^{-1} \left(\frac{M}{1\text{kton}}\right) \left(\frac{10\text{kpc}}{d}\right)^2 \\ &\int_{E_{\text{th}}}^{\infty} \left(\frac{\sigma(E)}{10^{-40}\text{cm}^2}\right) \left(\frac{\rho_{\alpha\alpha}(d)}{10^{58}\text{s}^{-1}\text{MeV}^{-1}}\right) \frac{dE}{\text{MeV}}. \end{aligned} \quad (24)$$

In calculating the reaction rates, we use the cross sections provided in Ref. [18] with necessary interpolations

⁵ This flux involves neutrinos going in all directions, not just the radial ones. To obtain the flux of only those neutrinos traveling radially, one should further divide this flux with another factor of π as shown in Ref. [27].

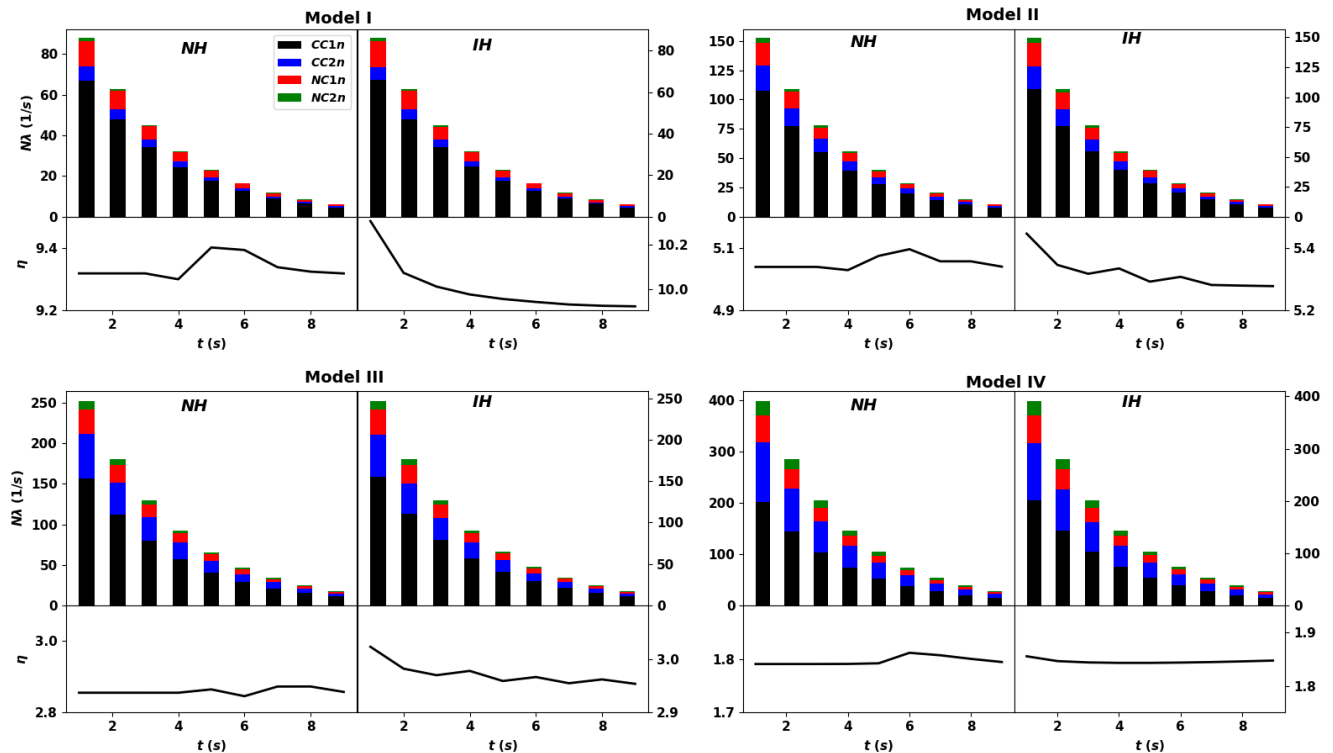


FIG. 7. Calculated reaction rates as functions of post-bounce time for models I-IV. Upper panels show the rates of CC1n, CC2n, NC1n, and NC2n reactions as indicated in the first panel. Lower panels show the ratio of 1n to 2n reaction rates. The left panels correspond to NH, and the right panels correspond to IH.

to our energy bins. The threshold energies of the reactions are calculated from measured masses and given in Table I. The density matrix elements $\rho_{\alpha\alpha}(d)$ are calculated by numerically evolving Eq. (5) through the relevant density profile at each second.

In HALO, the outgoing electron is not detected [65]. For this reason, CC and NC reactions cannot be distinguished from each other. But 1n and 2n events can be discriminated. Neither the detection nor the discrimination of 1n and 2n events is 100% efficient. But in our calculations, we assume perfect efficiency.

Fig. 7 shows the time dependent reaction rates that we calculate using Eq. (24) per 1 kt detector mass for a supernova which is 10 kpc away from the Earth. The left panels correspond to NH and the right panels correspond to IH. The upper panels show the individual rates of CC1n, CC2n, NC1n, and NC2n reactions. These reaction rates are also shown in Table II for NH and in Table III for IH. Note that the reaction rates we show in the tables are rounded to integer numbers whereas those plotted in Fig. 7 are not. The lower panels of Fig. 7 show the ratio of the total rate of 1n reactions to the total rate of 2n reactions, i.e.,

$$\eta(t) = \frac{\lambda_{CC1n}(t) + \lambda_{NC1n}(t)}{\lambda_{CC2n} + \lambda_{NC2n}(t)}. \quad (25)$$

Here, indices are used to refer to the rates of individual reactions. This ratio is independent from the detector size and from the distance of the supernova. If the effects of the shock wave and the changing character of collective oscillations are not considered, η would be independent of time. But even when these effects are taken into account, our results show that η depends only very weakly on time. For the models that we consider, we find that η changes by no more than a few percent with time for both NH and IH. The most substantial change is observed in model I in the case of IH where η drops from 10.3 to 9.9, which is about a 4% change. This tells us that the time dependent features that we consider here, i.e., the loss of sharpness in spectral splits with the decreasing neutrino luminosity, and the passage of the shock wave from the MSW resonance region, are likely to be lost within the error bars unless the statistics of the experiment is significantly improved.

As discussed above, there is a near degeneracy between NH and IH scenarios. In most cases, NH and IH results differ at most by a few events per second. But we find that, in each case, η is slightly larger for IH.

As we go from model I to model IV, all reaction rates increase. This is expected because $\langle E_{\nu_x} \rangle$ increases from model I to model IV. The energetic $\nu_\mu - \nu_\tau$ neutrinos are

	time (s)	1	2	3	4	5	6	7	8	9
Model I	CC1n	67	48	34	24	18	13	9	6	5
	NC1n	12	9	6	5	3	2	2	1	1
	CC2n	7	5	4	3	2	1	1	1	0
	NC2n	1	1	1	0	0	0	0	0	0
Model II	CC1n	108	77	55	40	28	20	15	10	7
	NC1n	19	14	10	7	5	4	3	2	1
	CC2n	21	15	11	8	6	4	3	2	1
	NC2n	4	3	2	1	1	1	1	0	0
Model III	CC1n	156	112	80	58	41	29	21	15	11
	NC1n	30	22	16	11	8	6	4	3	2
	CC2n	55	39	28	20	14	10	7	5	4
	NC2n	10	7	5	4	3	2	1	1	1
Model IV	CC1n	202	145	104	74	53	38	27	20	14
	NC1n	53	38	27	20	14	10	7	5	4
	CC2n	116	83	59	43	30	21	15	11	8
	NC2n	27	19	14	10	7	5	4	3	2

TABLE II. Calculated reaction rates (rounded to integers), in units of s^{-1} , for the case of NH as a function of time.

	time (s)	1	2	3	4	5	6	7	8	9
Model I	CC1n	66	47	34	24	17	12	9	6	5
	NC1n	12	9	6	5	3	2	2	1	1
	CC2n	6	5	3	2	2	1	1	1	0
	NC2n	1	1	1	0	0	0	0	0	0
Model II	CC1n	107	76	55	39	28	20	14	10	7
	NC1n	19	14	10	7	5	4	3	2	1
	CC2n	19	14	10	7	5	4	3	2	1
	NC2n	4	3	2	1	1	1	1	0	0
Model III	CC1n	155	110	79	57	41	29	21	15	11
	NC1n	30	22	16	11	8	6	4	3	2
	CC2n	51	37	27	19	14	10	7	5	4
	NC2n	10	7	5	4	3	2	1	1	1
Model IV	CC1n	201	143	103	74	53	38	27	19	14
	NC1n	53	38	27	20	14	10	7	5	4
	CC2n	110	79	57	41	29	21	15	11	8
	NC2n	27	19	14	10	7	5	4	3	2

TABLE III. Calculated reaction rates (rounded to integers), in units of s^{-1} , for the case of IH as a function of time.

converted to ν_e by collective oscillations in the case of IH and by the high resonances in the case of NH. But we also see that η decreases as we go from model I to model IV. This tells us that the 2n event rates increase to a greater extent with $\langle E_{\nu_x} \rangle$.

V. CONCLUSIONS

In this paper, we calculated the event rates in a lead-based detector due to a galactic core-collapse supernova. We paid particular attention to the time dependence of the reaction rates due to the flavor evolution of neutrinos through time dependent conditions in the supernova. In particular, we focused on the changing character of collective neutrino oscillations due to the decreasing neutrino luminosity, and the propagation of the shock wave through the MSW region.

For this purpose, we formed a one-dimensional supernova model by superimposing a parametric shock wave on a progenitor density distribution which models SN1987A. We considered four different models in this setting. These models have the same neutrino luminosities (which is consistent with SN1987A) but the initial neutrino energy distributions are different. In models I-III, we kept the ν_e and $\bar{\nu}_e$ distributions fixed while shifting ν_x distributions to higher energies. In model IV we used higher average energies for all flavors, which are far-fetched but not completely ruled out [53, 66].

For all models, we find that the sharpness of spectral splits decrease with time in the IH case. Since neutrinos do not go through high MSW resonance, this is the only source of time dependence in IH. However, we find that the resulting effect on reaction rates is limited because loss of sharpness becomes noticeable only when the neutrino luminosity drops considerably.

In the case of NH, neutrinos are not affected by collective oscillations but go through the high MSW resonance. In this case, the passage of the shock wave through the high MSW region is the only source of time dependence. Initially neutrinos experience only one high resonance but after the shock wave passes through this region, they start going through three high resonances. We find that the effects of the first two resonances mostly cancel each other, and the adiabaticity is only temporarily lost. For this reason, the resulting effect on the reaction rates is also limited.

All reaction rates decrease roughly exponentially as the neutrino luminosity drops. The ratio of 1n to 2n event rates is the best parameter to work with because it is independent of this overall decrease. We find that this ratio changes slightly with time due to the above-mentioned effects. In the case of IH, it slightly decreases with time. In the case of NH, it is initially constant, but later it changes as the shock wave passes through the high MSW resonance region. This effect is similar to the one observed in Ref. [43] for the electron antineutrino signal in water-Cherenkov detectors in the case of IH. However, in all the models that we looked at, the change is limited to a few percent. Therefore, it is likely to be lost within the error bars, or within the time dependence resulting the evolution of the proto-neutron star itself.

The evolution of the proto-neutron star is something that we intentionally left out in this paper. Our purpose was to isolate the time dependence resulting from the

dynamical flavor evolution of neutrinos outside the proto-neutron star. We also left out the multiangle nature of the collective neutrino oscillations. The multiangle effects delay the appearance of collective effects. They may also introduce angular decoherence and cause spectral splits to be less sharp, or even wash them out completely. For the type of initial spectra that we consider, in which ν_e and $\nu_\mu - \nu_\tau$ distributions cross each other only once, these effects appear to be minimal [48]. But in fact, the nature of the multiangle collective oscillations remains to be fully understood. See, e.g. Refs. [12, 67, 68]. At this point, we believe that their inclusion is not likely to change the

main results of this paper.

Y.P. thanks the APS Gordon and Betty Moore Foundation for their Visitor Award, which provided funding for a visit to University of Wisconsin-Madison (Grant no. GBMF6210). B. E. acknowledges the 2214A travel fellowship from the Scientific and Technological Research Council of Turkey (TÜBİTAK). Y.P. and B.E. thank to the University of Wisconsin-Madison their hospitality. This work was supported in part by TÜBİTAK under Project No. 117F327. The work of A. V. P. was supported in part by the NSF (Grant no. PHY-1630782) and the Heising-Simons Foundation (2017-228), and in part by the U.S. Department of Energy under contract number DE-AC02-76SF00515.

-
- [1] E. Cappellaro, R. Evans, and M. Turatto, *Astron.Astrophys.* **351**, 459 (1999), arXiv:astro-ph/9904225 [astro-ph].
- [2] R. Diehl, H. Halloin, K. Kretschmer, G. G. Lichti, V. Schoenfelder, *et al.*, *Nature* **439**, 45 (2006), arXiv:astro-ph/0601015 [astro-ph].
- [3] S. P. Reynolds, K. Borkowski, D. Green, U. Hwang, I. Harnus, and R. Petre, *Astrophys. J. Lett.* **680**, L41 (2008), arXiv:0803.1487 [astro-ph].
- [4] K. Scholberg, *Ann.Rev.Nucl.Part.Sci.* **62**, 81 (2012), arXiv:1205.6003 [astro-ph.IM].
- [5] H. Nagakura, *Mon. Not. Roy. Astron. Soc.* **500**, 319 (2020), arXiv:2008.10082 [astro-ph.HE].
- [6] S. Horiuchi and J. P. Kneller, *J. Phys. G* **45**, 043002 (2018), arXiv:1709.01515 [astro-ph.HE].
- [7] Z. Barkat, *Annual Review of Astronomy and Astrophysics* **13**, 45 (1975).
- [8] S. Woosley, A. Heger, and T. Weaver, *Rev.Mod.Phys.* **74**, 1015 (2002).
- [9] J. T. Pantaleone, *Phys.Rev.* **D46**, 510 (1992).
- [10] J. T. Pantaleone, *Phys.Lett.* **B287**, 128 (1992).
- [11] H. Duan, G. M. Fuller, and Y.-Z. Qian, *Ann.Rev.Nucl.Part.Sci.* **60**, 569 (2010), arXiv:1001.2799 [hep-ph].
- [12] S. Chakraborty, R. Hansen, I. Izaguirre, and G. Raffelt, *Nucl. Phys.* **B908**, 366 (2016), arXiv:1602.02766 [hep-ph].
- [13] L. Wolfenstein, *Phys.Rev.* **D17**, 2369 (1978).
- [14] S. Mikheev and A. Y. Smirnov, *Nuovo Cim.* **C9**, 17 (1986).
- [15] T.-K. Kuo and J. T. Pantaleone, *Rev.Mod.Phys.* **61**, 937 (1989).
- [16] K. Zuber, *Nuclear and Particle Physics Proceedings* **265-266**, 233 (2015), proceedings of the Neutrino Oscillation Workshop.
- [17] E. Kolbe and K. Langanke, *Phys. Rev. C* **63**, 025802 (2001), arXiv:nucl-th/0003060.
- [18] J. Engel, G. McLaughlin, and C. Volpe, *Phys. Rev. D* **67**, 013005 (2003), arXiv:hep-ph/0209267.
- [19] R. Lazauskas and C. Volpe, *Nucl. Phys. A* **792**, 219 (2007), arXiv:0704.2724 [nucl-th].
- [20] W. Almosly, B. Carlsson, J. Suhonen, J. Toivanen, and E. Ydrefors, *Phys. Rev. C* **94**, 044614 (2016).
- [21] W. Almosly, B. Carlsson, J. Suhonen, and E. Ydrefors, *Phys. Rev. C* **99**, 055801 (2019).
- [22] H. Ejiri, J. Suhonen, and K. Zuber, *Phys. Rept.* **797**, 1 (2019).
- [23] A. Gallo Rosso, (2020), arXiv:2012.12579 [hep-ph].
- [24] D. Vaananen and C. Volpe, *JCAP* **10**, 019 (2011), arXiv:1105.6225 [astro-ph.SR].
- [25] D. Vale, T. Rauscher, and N. Paar, *JCAP* **02**, 007 (2016), arXiv:1509.07342 [nucl-th].
- [26] A. Bandyopadhyay, P. Bhattacharjee, S. Chakraborty, K. Kar, and S. Saha, *Phys. Rev. D* **95**, 065022 (2017), arXiv:1607.05591 [astro-ph.HE].
- [27] H. Duan, G. M. Fuller, J. Carlson, and Y.-Z. Qian, *Phys.Rev.* **D74**, 105014 (2006), arXiv:astro-ph/0606616 [astro-ph].
- [28] H. Duan, G. M. Fuller, J. Carlson, and Y.-Z. Qian, *Phys. Rev. Lett.* **97**, 241101 (2006), arXiv:astro-ph/0608050.
- [29] G. G. Raffelt and A. Y. Smirnov, *Phys.Rev.* **D76**, 081301 (2007), [Erratum-ibid. *D* **77**, 029903 (2008)], arXiv:0705.1830 [hep-ph].
- [30] G. G. Raffelt and A. Y. Smirnov, *Phys.Rev.* **D76**, 125008 (2007), arXiv:0709.4641 [hep-ph].
- [31] H. Duan, G. M. Fuller, J. Carlson, and Y.-Z. Qian, *Phys. Rev. Lett.* **99**, 241802 (2007), arXiv:0707.0290 [astro-ph].
- [32] B. Dasgupta, A. Mirizzi, I. Tamborra, and R. Tomas, *Phys. Rev. D* **81**, 093008 (2010), arXiv:1002.2943 [hep-ph].
- [33] S. Choubey, B. Dasgupta, A. Dighe, and A. Mirizzi, (2010), arXiv:1008.0308 [hep-ph].
- [34] T. Fischer, S. Whitehouse, A. Mezzacappa, F.-K. Thielemann, and M. Liebendorfer, *Astron. Astrophys.* **517**, A80 (2010), arXiv:0908.1871 [astro-ph.HE].
- [35] A. Mirizzi, I. Tamborra, H.-T. Janka, N. Saviano, K. Scholberg, R. Bollig, L. Hudepohl, and S. Chakraborty, *Riv. Nuovo Cim.* **39**, 1 (2016), arXiv:1508.00785 [astro-ph.HE].
- [36] L. F. Roberts and S. Reddy, (2016), arXiv:1612.03860 [astro-ph.HE].
- [37] R. C. Schirato and G. M. Fuller, (2002), arXiv:astro-ph/0205390 [astro-ph].
- [38] G. L. Fogli, E. Lisi, A. Mirizzi, and D. Montanino, *Phys. Rev.* **D68**, 033005 (2003), arXiv:hep-ph/0304056 [hep-ph].
- [39] K. Takahashi, K. Sato, H. E. Dalhed, and J. R. Wilson, *Astropart. Phys.* **20**, 189 (2003), arXiv:astro-ph/0212195.
- [40] R. Tomas, M. Kachelriess, G. Raffelt, A. Dighe, H. T.

- Janka, and L. Scheck, JCAP **0409**, 015 (2004), arXiv:astro-ph/0407132 [astro-ph].
- [41] B. Dasgupta and A. Dighe, Phys. Rev. D **75**, 093002 (2007), arXiv:hep-ph/0510219.
- [42] A. Friedland and A. Gruzinov, (2006), arXiv:astro-ph/0607244.
- [43] J. Gava, J. Kneller, C. Volpe, and G. C. McLaughlin, Phys. Rev. Lett. **103**, 071101 (2009), arXiv:0902.0317 [hep-ph].
- [44] A. Friedland and P. Mukhopadhyay, (2020), arXiv:2009.10059 [astro-ph.HE].
- [45] B. Pointon, in *XXVIII International Conference on Neutrino Physics and Astrophysics* (2018) p. 474.
- [46] C. Virtue, private communication.
- [47] G. Sigl and G. Raffelt, Nucl.Phys. **B406**, 423 (1993).
- [48] A. Mirizzi and R. Tomas, Phys. Rev. D **84**, 033013 (2011), arXiv:1012.1339 [hep-ph].
- [49] W. D. Arnett, J. N. Bahcall, R. P. Kirshner, and S. E. Woosley, Annual Review of Astronomy and Astrophysics **27**, 629 (1989), <https://doi.org/10.1146/annurev.aa.27.090189.003213>.
- [50] T. Yoshida, M. Terasawa, T. Kajino, and K. Sumiyoshi, Astrophys. J. **600**, 204 (2004), arXiv:astro-ph/0305555.
- [51] H. Suzuki, in *Physics and Astrophysics of Neutrinos*, edited by M. Fukugita and A. Suzuki (1994) pp. 763–847.
- [52] M. T. Keil, G. G. Raffelt, and H.-T. Janka, Astrophys.J. **590**, 971 (2003), astro-ph/0208035.
- [53] G. J. Mathews, J. Hidaka, T. Kajino, and J. Suzuki, Astrophys.J. **790**, 115 (2014), arXiv:arXiv: 1405.0458 [astro-ph.CO].
- [54] P. Zyla *et al.* (Particle Data Group), PTEP **2020**, 083C01 (2020).
- [55] V. Barger, K. Whisnant, S. Pakvasa, and R. J. N. Phillips, Phys. Rev. D **22**, 2718 (1980).
- [56] K. Nomoto, T. Shigezawa, and M.-A. Hashimoto, in *European Southern Observatory Conference and Workshop Proceedings*, European Southern Observatory Conference and Workshop Proceedings, Vol. 26, edited by I. J. Danziger (Garching bei München, Germany, 1987) pp. 325–346.
- [57] G. M. Fuller, R. W. Mayle, J. R. Wilson, and D. N. Schramm, Astrophys. J. **322**, 795 (1987).
- [58] M. J. Savage, R. A. Malaney, and G. M. Fuller, Astrophys. J. **368**, 1 (1991).
- [59] A. B. Balantekin, J. Gava, and C. Volpe, Phys.Lett. **B662**, 396 (2008), arXiv:0710.3112 [astro-ph].
- [60] J. Gava and C. Volpe, Nucl.Phys. **B837**, 50 (2010), arXiv:1002.0981 [hep-ph].
- [61] J. P. Kneller and G. C. McLaughlin, Phys.Rev. **D80**, 053002 (2009), arXiv:0904.3823 [hep-ph].
- [62] J. Gava and C. Volpe, Phys.Rev. **D78**, 083007 (2008), arXiv:0807.3418 [astro-ph].
- [63] H. Yokomakura, K. Kimura, and A. Takamura, Physics Letters B **544**, 286 (2002), arXiv:hep-ph/0207174 [hep-ph].
- [64] Y. Pehlivan, A. Balantekin, and T. Kajino, Phys.Rev. **D90**, 065011 (2014), arXiv:1406.5489 [hep-ph].
- [65] M. A. Schumaker *et al.*, in *2010 IEEE Nuclear Science Symposium, Medical Imaging Conference, and 17th Room Temperature Semiconductor Detectors Workshop* (2010) pp. 1860–1865.
- [66] A. Mezzacappa, M. Liebendoerfer, O. B. Messer, W. Hix, F.-K. Thielemann, and S. W. Bruenn, Phys. Rev. Lett. **86**, 1935 (2001), arXiv:astro-ph/0005366.
- [67] S. Chakraborty, A. Mirizzi, N. Saviano, and D. d. S. Seixas, Phys. Rev. D **89**, 093001 (2014), arXiv:1402.1767 [hep-ph].
- [68] T. Morinaga, H. Nagakura, C. Kato, and S. Yamada, Phys. Rev. Res. **2**, 012046 (2020), arXiv:1909.13131 [astro-ph.HE].